

Effect of bed roughness on tsunami bore propagation and overtopping

Esteban, Miguel; Roubos, Jochem Jan; Imura, Kotaro; Salet, Jorrit Thomas; Hofland, Bas; Bricker, Jeremy; Ishii, Hidenori; Hamano, Go; Takabatake, Tomoyuki; Shibayama, Tomoya

DOI

[10.1016/j.coastaleng.2019.103539](https://doi.org/10.1016/j.coastaleng.2019.103539)

Publication date

2020

Document Version

Accepted author manuscript

Published in

Coastal Engineering

Citation (APA)

Esteban, M., Roubos, J. J., Imura, K., Salet, J. T., Hofland, B., Bricker, J., Ishii, H., Hamano, G., Takabatake, T., & Shibayama, T. (2020). Effect of bed roughness on tsunami bore propagation and overtopping. *Coastal Engineering*, 157, Article 103539. <https://doi.org/10.1016/j.coastaleng.2019.103539>

Important note

To cite this publication, please use the final published version (if applicable).
Please check the document version above.

Copyright

Other than for strictly personal use, it is not permitted to download, forward or distribute the text or part of it, without the consent of the author(s) and/or copyright holder(s), unless the work is under an open content license such as Creative Commons.

Takedown policy

Please contact us and provide details if you believe this document breaches copyrights.
We will remove access to the work immediately and investigate your claim.

1
2 **EFFECT OF BED ROUGHNESS ON TSUNAMI BORE PROPAGATION AND**
3 **OVERTOPPING**

4 **Miguel Esteban¹, Jochem Jan Roubos², Kotaro Iimura¹, Jorrit Thomas Salet², Bas Hofland²,**
5 **Jeremy Bricker², Hidenori Ishii¹, Go Hamano¹, Tomoyuki Takabatake¹, Tomoya**
6 **Shibayama¹**

- 7
8 1. Dept. Civil and Environmental Engineering, Waseda University, 3-4-1 Ookubo, Tokyo, 169-8555, Japan.
9 2. Dept. of Hydraulic Engineering, Faculty of Civil Engineering and Geosciences, Delft University of
10 Technology, Stevinweg 1, 2628CN Delft, Netherlands
11 .
12
13

14 **Abstract**

15 The accurate modelling of overtopping of coastal defences by tsunami waves is of vital
16 importance for the formulation of disaster management strategies. To improve knowledge
17 of this phenomena the authors conducted experiments on coastal structure overtopping
18 using bores that were generated by a dam-break mechanism. Three types of structures
19 were tested, namely a coastal dyke, a wall, and a wall of infinite height. The results
20 highlight the necessity to consider the energy present in a bore to determine if a structure
21 will be overtopped or not. As a result of these experiments an empirical formula to
22 determine the height of overtopping given the incident bore height and velocity was
23 validated. The study highlights the importance of clearly modelling the velocity and
24 Froude number of a tsunami. Such experiments should be conducted on rough beds, for
25 which a suitable Manning's n seems to be around $0.06 \text{ sm}^{-1/3}$. The study also contrasted
26 the results obtained to those of the ASCE7 method, and concludes that the Manning's n
27 values recommended in ASCE7 are probably too low.
28
29

30 **Keywords:** tsunami overtopping; evacuation; dam break; dykes
31
32

33

34 1. INTRODUCTION

35

36 Tsunamis can devastate large portions of the coastline, inflicting severe casualties to any
37 community situated on it that is not adequately prepared. To counteract these events, concrete
38 structures have been built along large sections of coastlines at risk, particularly in the case of
39 Japan. Despite the presence of such structures, the *2011 Tohoku Earthquake and Tsunami*
40 (which generated run-ups of 10 to 40 m along the Tohoku coastline, Mori et al., 2011), went
41 on to inflict casualties that sometimes exceeded 10% of the resident population (Yamao et al.,
42 2015). Almost 20,000 people lost their lives in total, between those dead and still missing
43 (The Japan Times, March 8, 2016), and 169 bn USD of assets were ~~lots~~-lost (equivalent to
44 approximately 3% of the country's GDP (Japanese Cabinet Office, 2011; Ranghieri and
45 Ishiwatari, 2014).

46

47 The failure of what was considered at the time a modern countermeasure system (Mori et al.,
48 2011) has led to a re-assessment of the role of "hard" structures in tsunami disaster mitigation.
49 Particularly, engineers have been trying to draw lessons about why some structures were
50 overtopped but others were not. In areas where a bore might not have possessed enough
51 energy only minor flooding was recorded behind the structures, such as in the case of Fudai.
52 In this town floodgates and dykes were effective at dissipating the tsunami's energy, even
53 though the structure was eventually partly overtopped (Fig. 1, left). However, throughout
54 most of the coastline the defences were not high enough, and the wave carried enough energy
55 to overtop them and destroy the town behind them (such as at Taro, for example, Fig. 1, right).

56

57



58

59 Figure 1. Left: The dyke and floodgates at Fudai successfully stopped the tsunami, despite
60 suffering some overtopping (inundation marks of ~20m in front of the structure, indicated by

61 the blue sign on the rightmost tower). Right: At Taro the massive coastal walls were
62 overtopped, and the town behind them completely destroyed (pictures by authors).

63

64 Following the 2011 event the Japanese coastal engineering community has started to classify
65 tsunamis into two different levels, depending on their severity and intensity (Shibayama et al.,
66 2013). Level 1 events would have a return period of several decades to around 100 years, and
67 would result in smaller inundation heights than Level 2 events. Level 2 events would have
68 return periods of a few hundred to a few thousand years, and for the case of substantial parts
69 of the Japanese coastline would have inundation heights in excess of 10 m (Shibayama et al.,
70 2013). The *2011 Tohoku Earthquake and Tsunami* is considered a Level 2 event, given that it
71 has a return period greater than 1 in 1,000 years, though the tsunami height levels are
72 calculated at each point of the coastline according to historical data on tsunami return periods.
73 While there is some uncertainty on these, this change in philosophy essentially represents a
74 move by Japanese disaster risk management to move to a probabilistic management of
75 tsunami risk.

76

77 The determination of the tsunami level is crucial when it comes to the design of tsunami
78 countermeasures. “Hard measures”, such as breakwaters or coastal protection dykes, should
79 be sufficiently high to protect residents and their property in the case of a Level 1 event. For
80 the case of Level 2 events it is accepted that coastal defences would be overtopped, and that
81 residents would have to rely on “soft measures”, such as evacuation to higher ground or
82 tsunami shelters. However, even in this case hard measures are expected to survive the event,
83 and should play a secondary role in slowing the advance of the tsunami and providing
84 residents with extra time to evacuate (Tomita et al., 2012). For example, in the case of
85 Otsuchi town, in Iwate prefecture, prior to the 2011 event the highest tsunami walls were built
86 up to a height of +6.4 m T.P.¹. Simulations carried out by the national and prefectural
87 governments indicate that the 1896 *Meiji-Sanriku* tsunami should become the benchmark for
88 a Level 1 event (which required tsunami walls to be a level of +10.5 m T.P.) (Iwate Prefecture
89 Tsunami Disaster Prevention Technical Committee 2013). However, as the town is located
90 close to Kamaishi city it was decided that most of the tsunami walls would be built to the
91 same inundation height as that expected in Kamaishi, i.e. to a level of +14.5 m T.P (see
92 Figure 2, top left). Simulations indicate that even for such a wall partial overtopping is
93 possible, allowing some water to flood the land behind it (Esteban et al., 2015). While the
94 land behind the dykes has also been raised (Figure 2, top right), it is necessary to understand

¹ These heights are presented relative to Tokyo Peil (T.P. corresponds to mean sea level of Tokyo Bay).

95 to what extent the new dyke will be successful at stopping inundation behind it. Other similar
 96 dykes are being rebuilt elsewhere along the coastline (see Figure 2, bottom)



Figure 2. Top left. Construction of new dyke in Otsuchi town (Sept 2018). Top right. New park in Otsuchi, showing the original level of the town (pond on the right) and the new level (houses at the back). Bottom left. Reconstructed dike along the Sendai plains coastline (photo courtesy of Glasbergen, T). Bottom right. New coastal dyke at Rikuzentakata, in front of a preserved memorial building.

105 In the aftermath of the 2011 event many field survey reports have ~~analyzed~~analysed the types
 106 of failure mechanisms of coastal structures (Kato et al., 2012; Mikami et al., 2012; Mori and
 107 Takahashi, 2012; Jayaratne et al., 2016; Esteban et al., 2014). It is evident that beach
 108 bathymetry, coastal geomorphology, onshore coastal topography, coastal structure geometry
 109 and tsunami wave conditions, influence the failure modes and mechanisms of coastal
 110 structures (Kato et al., 2012; Mikami et al., 2013; Jayaratne et al., 2016). For the case of
 111 dykes, a number of authors (Kato et al., 2012; Mikami et al., 2013; Jayaratne et al., 2016)
 112 identified how leeward toe scour was the leading failure mechanism, though a number of
 113 other types of mechanisms could also be observed (Bricker et al., 2012; Kato et al., 2012;
 114 Tonkin et al., 2014; Jayaratne et al., 2016). Essentially, most structures were insufficiently
 115 strong to withstand the lateral and overtopping pressures and forces exerted on them, as they
 116 were based on research on solitary waves that had mostly not contemplated overtopping (see
 117 Tanimoto et al., 1984; Ikeno et al., 2001, 2003; Mizutani and Imamura, 2000; Esteban et al.,
 118 2008, 2009, 2016). However, following the 2011 event the use of solitary waves in tsunami
 119 modelling has been questioned, due to the relatively short distance between the source region
 120 and coast, compared to the distance in which a soliton forms (Madsen et al., 2008). Due to

121 this, many researchers nowadays accept that the use of solitary waves can only be considered
122 to reproduce the ~~incipient motion~~ first stage of a tsunami wave as it reached the coastline of
123 ~~the tsunami wave~~ (Goseberg et al., 2013). Hence, in recent times other researchers have
124 focused on the current velocity and overtopping effects to design armour of breakwaters
125 against tsunami attack (Sakakiyama, 2012; Hanzawa et al., 2012; Kato et al., 2012), even
126 though it is difficult to accurately replicate such effects in the lab.

127

128 It is important to note how, despite failing, protection structures might have played a role in
129 mitigating tsunami damage (Nateghi et al., 2016), as highlighted by field surveys (Mikami et
130 al., 2012; Suppasri et al., 2012; EERI, 2011; Omira et al., 2013; Latcharote et al., 2016) and
131 numerical simulations (Nandasena et al., 2012; Stansby et al., 2008; Hunt-Raby et al., 2011).
132 One of the more significant of such structures was the Kamaishi tsunami breakwater, the
133 deepest breakwater built anywhere in the world. Following the disaster, Tomita et al. (2012)
134 conducted simulations that show that the structure could have reduced inundation heights in
135 Kamaishi city from 13.7 m to 8.0 m, providing residents an extra 6 minutes to evacuate
136 (though the effect of damaged sections of this breakwater was neglected in the calculations of
137 tsunami approach time, Cyranoski, 2012). However, other more typical breakwaters were
138 basically designed to reflect wind waves, and the reduction of the tsunami impact due to them
139 should also not be overestimated (Takagi and Bricker, 2014).

140

141 Thus, the 2011 event triggered an abundance of research dealing with the stability of tsunami
142 countermeasures, though comparatively little experimental research has been conducted on
143 understanding the overtopping of tsunami-induced flows over tsunami walls or dykes. To
144 properly understand the benefits of coastal structures that are overtopped, as is expected for
145 Level 1 tsunamis, it is important to determine the volume of water, flooding depth (d_f) and
146 velocity (v) that can result from an overtopping tsunami. The $d_f \cdot v$ product is particularly
147 important, as values higher than 0.5 m²/s can result in 50% mortality, which increases to
148 almost 100% when $d_f \cdot v > 2$ m²/s (Jonkman and Penning-Rowsell, 2008). If correctly
149 designed, these structures can play a critical role in lowering this $d_f v$ value, and provide
150 residents with extra time to evacuate (Okumura et al., 2017; Takabatake et al., 2017, 2018).
151 Coupled with improved evacuation procedures and communication, such disaster
152 management systems would make it easier for residents and visitors to an area evacuate in the
153 case of a tsunami (San Carlos-Arce et al., 2017).

154

155 As a result, Esteban et al (2017) set out to investigate overtopping flow patterns that result
156 from a variety of different incident bore-type conditions. The laboratory experiments detailed

157 by these authors were then followed by detailed computer simulations by Glasbergen (2018),
158 using a bathymetry that attempted to simulate typical beach profiles along the Sendai planes,
159 in the northern Tohoku region in Japan. The results of Esteban et al. (2017) and Glasbergen
160 (2018) showed that whether a structure is overtopped or not will depend on the energy in the
161 bore, with lower velocity bores less likely to overtop a structure than higher velocity ones.

162

163 However, the experiments of Esteban et al. (2017) suffered from the limitation of only having
164 been carried out on a smooth bed, and thus did not take into account the effect of different
165 (and more realistic) bed roughness coefficients. Furthermore, it is not clear whether the high
166 velocities and Froude numbers obtained using a dry bed are truly representative of a tsunami-
167 like flow. Thus, in the present work the authors set out to address this problem by conducting
168 a new set of experiments on a rough bed, which were then compared to the original results
169 detailed in Esteban et al. (2017). The authors then provide some guidelines as to how high a
170 structure would have to be so that it can effectively help in the evacuation of citizens against a
171 Level 2 tsunami.

172

173 However, tsunamis can also represent a threat to coastal communities outside Japan. The
174 ASCE7 (ASCE 2016) became the first North American standard that is written in mandatory
175 language, addressing tsunami hazards and how these apply to the context of North America
176 (Stolle et al., 2019). The International Building Code (IBC) references design provisions that
177 are provided for in the ASCE7 Standard, and thus has become part of an enacted building
178 code law through adoption of the model International Building Code by the state, county, or
179 city (Chock, 2015). This guideline contains a simplified method (called the Energy Grade
180 Line, or EGL, method) to establish maximum tsunami inundation depth and flow speed
181 values, based on inundation maps throughout the United States. The present research will also
182 attempt to validate the accuracy of such a model, in light of the laboratory experiments carried
183 out in the present work, and the simulations conducted by Glasbergen (2018).

184

185 2. EXPERIMENTAL PROGRAM

186

187 Two different rounds of laboratory experiments (in Sept 2017 and Sept-Oct 2018) using a
188 dam break generation mechanism were performed in a wave flume (dimensions 14 m × 0.41
189 m × 0.6 m) at Waseda University, Tokyo, Japan. The first analyses of the 2017 smooth-bed
190 tests was given by Esteban et al. (2017). Froude scaling of 1:50 was used when converting the
191 velocity of the bore to real-life conditions, to see how accurately the wave resembled that of a

192 real life tsunami event. A schematic representation of the wave tank and the apparatus in it,
193 as used for both tests series, is shown in Fig. 3. On the left side of the tank a dam break
194 generation mechanism was operated by a system of pulleys attached to a heavy weight (See
195 Fig. 4). The opening height of the gate was 15 cm. As the weight was not changed throughout
196 the experiments, the gate opening speed also remained constant. Behind this gate a 4.5 m
197 reservoir ensured that there was enough water to generate a long bore (water levels behind the
198 gate varied between experimental cases, meaning that between 18.9 and 37.8 m³ of water
199 were released each time). In total, 12 experimental cases were carried out, for water levels in
200 the reservoir of $d = 30, 40, 50$ and 60 cm, and water levels in front of the reservoir of $h = 0,$
201 10 and 20 cm.

202

203 (PLEASE SEE FIGURE 3 AT END OF THIS DOCUMENT)

204

205 (PLEASE SEE FIGURE 4 AT END OF THIS DOCUMENT)

206

207

208 A metal false bed was constructed on top of the floor of the tank, with the start of the sloping
209 section being only 5 cm away from the edge of the gate. The horizontal section of the false
210 bed was 20 cm above flume bed, with the slope of the initial section being 1:10. All of the
211 experimental cases were repeated for two false bed conditions. The first was the smooth metal
212 finish of the actual bed. For the second condition, acrylic layers were fixed on top of the false
213 bed, with small diameter stones (3-5mm, corresponding to a Manning $n = 0.02 \text{ sm}^{-1/3}$
214 according to Limerinos, 1970) being glued to the entire face of each of the panels. This made
215 the bed in the rough bed case slightly (ca. 5 mm) higher. Note that there are more physically
216 realistic ways than Manning's n to parameterize bed roughness (see for example the
217 discussion at the end of Bricker et al., 2015), but Manning's n still pervades the practice of
218 inundation modeling and is encoded by the ASCE7, so it is thus the focus of the present study.

219

220 The test section was located 1.65 m away from the top end of the sloping part of the false
221 bottom, with three different structures being tested: (1) a coastal dyke, (2) a low tsunami wall
222 and (3) a high tsunami wall (this wall was not overtopped, so it can be regarded as a wall of
223 "infinite height"). The dyke was constructed using a combination of acrylic panels and a
224 hollow metallic structure (9.5 cm high, 26 cm long across the base and 6cm wide at the top,
225 see Fig. 5). The low tsunami wall was essentially one concrete block 15 cm high and 10 cm
226 wide (Fig. 5). The high tsunami wall consisted on a 39 cm high acrylic panel, supported at the
227 base by a concrete brick (Fig. 5). The false bed and all of the test structures were fixed to the

228 sides of the wave tank using silicon, and particular attention was paid to them being
229 completely sealed. No movement was observed in any of the structures or false bed during the
230 experiments. At the end of the tank a wave absorption beach was constructed, under which
231 there was a drain that allowed for excess water to be removed after each experiment.

232

233 (PLEASE SEE FIGURE 5 AT END OF THIS DOCUMENT)

234

235 Several wave gauges (WG) and velocity meters (VM) were placed in the tank, as shown in
236 Fig. 1. All gauges (KENEK CHT6–30, 40) were of the capacitance type, with a range of
237 either 30 or 40 cm. Table 1 shows a summary of the experimental conditions (note that some
238 definitions in the table will be further elaborated in the results section). To evaluate the
239 hydrodynamic conditions of the waves that were generated experiments were also performed
240 without any structures being present inside the tank, focusing on the unobstructed water
241 surface elevation and velocity profile just before the test area. The instruments used a data
242 logging system (KENEK ADS2016), which was connected to a PC. The sampling frequency
243 of all measurements was 200 Hz. A high-speed Nikon D5200 camera (60 frames per second)
244 was mounted on a tripod, directly in front of the structures. This allowed the analysis of the
245 profile of the bores as they hit the structures, and the overflowing patterns that resulted from
246 them.

247

248 The velocity meters (KENEK VMT2–200–04P, 04PL) used in the experiment were all
249 electromagnetic current meters (ECMs), with a range of measurement of 2 m/s. A low pass
250 filter of 20 Hz was applied after the data acquisition. They were placed at the top of the
251 structure and 15 cm behind it, to attempt to measure the overtopping conditions. However,
252 due to air bubbles entrained within the turbulent bore and disturbance of the free surface due
253 to the high-speed flow around the probe head, the complete velocity profile could not be
254 accurately recorded for the entire length of the experiments. Thus, the measurements obtained
255 by this type of instrumentation were considered to be approximate reference values, and the
256 bore front velocities were measured from the wave gauge (WG) data, as will be discussed
257 later.

258

259 In preparation for each of the experimental cases the tank was drained and filled to the
260 specified height with water (both for the case of the water in the reservoir and that in the main
261 test section). It should be noted that wet bed conditions were used in all experimental

262 conditions. To ensure replicability certain experimental conditions were repeated five times,
263 as will be discussed later in this paper.

264

265 $T/2$ (the “wave half-period” of the “tsunami-like wave”) was estimated from the wave profile
266 of the experimental cases where no structure was present in the tank. For the experimental
267 cases with less water, $T/2$ could be calculated precisely (For example, for the smooth bed
268 experiments $T/2 = 10.6$ s for $d=30$ cm and $h=0$ cm, which would correspond to a real life $T/2$
269 $= 74.9$ s). However, as the amount of water in the reservoir was increased the wave was
270 faster and it reached the end of the tank and was reflected before a full cycle could be
271 recorded. Thus, it was only possible to conclude that, $T/2 > 16.1$ for $d=60$ cm and $h=0$ cm for
272 the smooth bed corresponding to a real life tsunami $T/2 > 113.8$ s. For the case of the rough
273 bed, the wave appeared to advance slower, and for $d=30$ cm a secondary wave (reflected from
274 the sloped section onto the gate and back onto the structure) reached the test section before a
275 full cycle was finished. Thus, it was only possible to conclude that $T/2 > 12.18$ s for $d=30$ cm
276 and $h=0$ cm and $T/2 > 14.12$ s for $d=60$ cm and $h=0$ cm for the rough bed (real life $T/2$ of 86.1
277 and 99.8 s, respectively). Despite this limitation, a $T/2 > 10$ s meant that the experiments were
278 able to reach a quasi-stationary overtopping flow (for the experimental cases where
279 overtopping took place), which could be considered similar to what was observed during the
280 *2011 Tohoku Earthquake and Tsunami*.

281

282 Table 1. Summary of experimental conditions and results (note that some of the mentioned
 283 variables will be defined in the results section). Numbers in bold italics indicate the
 284 experimental conditions ($d=50$, $h=0$ cm, for both the low vertical wall and the dyke) that were
 285 repeated 5 times. Results for the smooth bed case are repeated from Esteban et al. (2017).

Rough Bed		Structure Type									
		Water depth in reservoir / in front of the reservoir		No structure		High vertical wall (non-overtopped)	Low vertical wall			Dyke	
d [cm]	h [cm]	H_i [cm] <i>WG5</i>	V_i [m/s] <i>WG2-4</i>	H_{f0} [cm] <i>WG3</i>	H_f [cm] <i>WG3</i>	H_o [cm] <i>WG5</i>	H_b [cm] <i>WG6</i>	H_f [cm] <i>WG3</i>	H_o [cm] <i>WG5</i>	H_b [cm] <i>WG6</i>	
No	30	0	3.42	1.24	8.24	8.57	0	0	8.06	0.41	1.43
		10	3.67	1.15	7.79	7.15	0	0.02	8.57	0	0.61
		20	3.73	0.88	8.2	7.49	0	0.02	8.7	0.04	0.12
	40	0	5.49	1.68	16.15	15.21	0.9	1.48	13.73	5.55	4
		10	5.64	1.37	14.59	14.46	0.21	1.41	13.39	4.41	2.4
		20	5.64	1.79	15.41	14.85	0.57	1.62	13.58	3.89	2.58
	50	0	8.59	2.12	24.3	21.04	10.76	5.31	17.61	11.35	7.56
		10	7.79	1.92	22.38	19.28	4.92	3.26	17.11	9.22	6.88
		20	8.32	1.66	21.41	20.16	5.31	4.3	17.97	10.45	7.38
	60	0	12.17	2.59	33.69	27.55	16.33	9.45	20.32	16	9.92
		10	10.74	2.43	28.61	24.35	11.11	6.95	20.36	13.16	8.95
		20	10.27	2.7	28.63	24.17	12.38	6.88	20.89	13.48	10.12
Yes	30	0	3.38	0.99	8.59	8.81	0.03	0.04	7.62	0	0
		10	3.11	0.86	7.44	6.89	0	0	7.48	0	0
		20	3.28	0.78	8.32	7.38	0.03	0.04	8.01	0	0
	40	0	5.63	1.36	18.13	16.07	0.32	0.62	15.27	5.19	2.61
		10	5.23	1.28	16.46	14.18	0.28	0.03	13.87	2.99	2.02
		20	5.86	1.29	17.66	16.13	0.72	1.99	13.85	3.22	2.21
	50	0	7.95	1.82	25.98	21.59	6.518	3.784	19.138	9.234	4.844
		10	7.5	1.49	24.08	22.54	4.1	3.69	18.09	7.22	4.2
		20	8.01	1.27	26.35	21.88	7.63	2.61	18.4	11.06	3.37
	60	0	10.55	1.96	33.55	28.38	12.29	7.15	24.34	13.67	8.13
		10	9.96	1.65	32.95	35.55	10.27	6.24	21.21	12.08	7.6
		20	10.76	1.42	32.38	31.45	11.65	4.66	21.43	12.38	6.09

287

288 **3. RESULTS**

289

290 3.1. Experiment repeatability

291

292 When performing tests using dam-break experiments it is important to ascertain whether tests
 293 are consistent. Esteban et al. (2017) proved this by repeating experiments 5 times for the case
 294 of the “low tsunami wall” and “dyke” structure experiments with $d = 50$ cm and $h = 0$ cm
 295 (showed in bold italics in Table 1). For the case of the rough bed the coefficient of variation
 296 from the averaged maximum water level recorded at each gauge was low, as shown in Table 2.
 297

298 However, the measurements by the velocity metres were much less consistent, for both the
 299 rough and smooth bed conditions. In this sense, the present experiments were unable to
 300 improve on the methodology of Esteban et al. (2017) and were thus omitted (the velocity
 301 meters are electromagnetic instruments that do not produce reliable results in conditions of
 302 substantial air entrainment).

303

304 Table 2. Summary of the coefficient of variation for the various experiments conditions, for
 305 $d=50$ cm and $h=0$ cm (based on 5 experiments)

Structure	Bed type	WG1	WG3	WG5	WG6
Low Vertical Wall	Smooth bed	1.2%	1.9%	13.5%	10.6%
	Rough bed	3.8%	0.6%	12.0%	6.3%
Dyke	Smooth bed	1.2%	1.7%	4.8%	6.3%
	Rough bed	1.0%	4.2%	6.9%	5.3%

306

307

308

309 3.2. Dam break Wave Profile

310

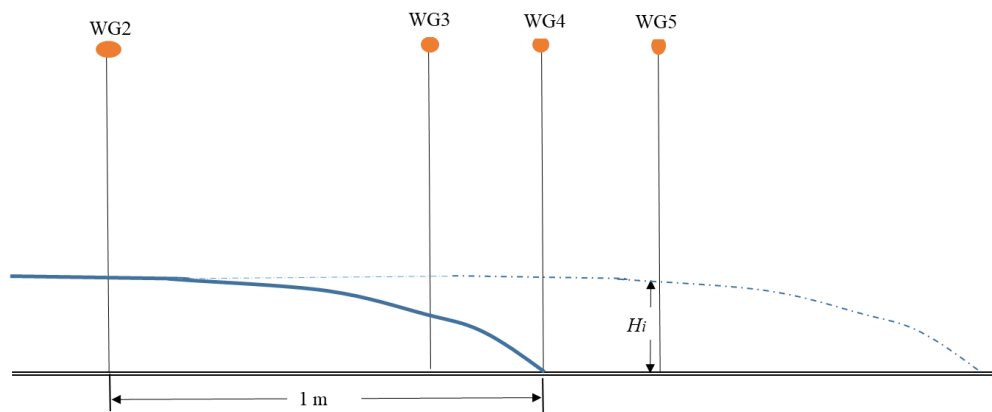
311 As stated earlier it was difficult to get accurate readings from the velocity metres, as the
 312 velocity of the incident bores typically exceeded their capabilities (full range of 2 m/s), and
 313 the entrapment of air behind the probes resulted in missing data points (also reported in
 314 Esteban et al., 2017). To overcome this problem, the authors used the bore front velocity to
 315 approximate the maximum kinetic energy present in the wave-like flow (following Dressler,
 316 1954; Estrade and Martinot, 1964; and Chanson, 2006, who estimated that the flow velocity
 317 in the turbulent bore tip is roughly equal to the bore front velocity). As the experiments were

318 conducted over a horizontal, flat, unobstructed surface, the bore front velocity should
 319 represent the maximum velocity of the flow.

320

321 Following Esteban et al. (2017), the bore front velocity was thus calculated by measuring the
 322 time for the bore tip to travel between WG2 and WG4 (which were situated 1.0 m apart from
 323 each other) when no structure was present in the tank (see Fig. 6). The incident wave height
 324 (H_i) was considered to be the maximum height of the wave as it traversed WG5 (as this was
 325 the location of the centre of the structures in the other experimental cases), with Table 1 also
 326 showing the values of V_i . When no structures were present the bore appeared uniform as it
 327 made progress over the false bed (i.e. there appeared to be no change in its profile between
 328 WG4 and WG5, see Fig 6). This obviously changed when the structures were placed inside the
 329 tank, as the wave crashed into the structure and overtopped it (if it had sufficient kinetic
 330 energy).

331



332

333 Fig. 6. Diagrammatic representation of the calculation of the bore velocity V_i . The continuous
 334 line indicates the wave profile as the bore reaches WG4. H_i , the incident (unobstructed) wave
 335 height, was taken as the maximum water level at WG5 (with the discontinuous line showing
 336 the wave profile at this moment).

337

338 The notional Froude number Fr for the bore front given in Fig. 6 is defined by equation (1),

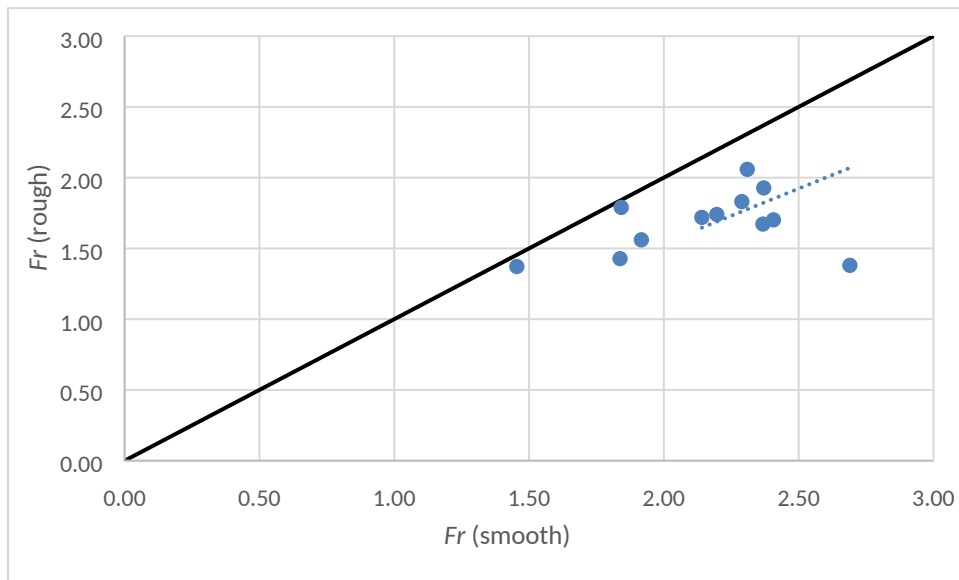
339

$$340 \quad Fr = \frac{V_i}{\sqrt{gH_i}} \quad (1)$$

341

342 It is important to remember that this Fr is not the steady flow Froude number, given that this
 343 is a front propagating over a dry bed, and that the front velocity and (maximum) flow depth
 344 are measured at different times. The Fr for the rough bed and smooth bed experiments was

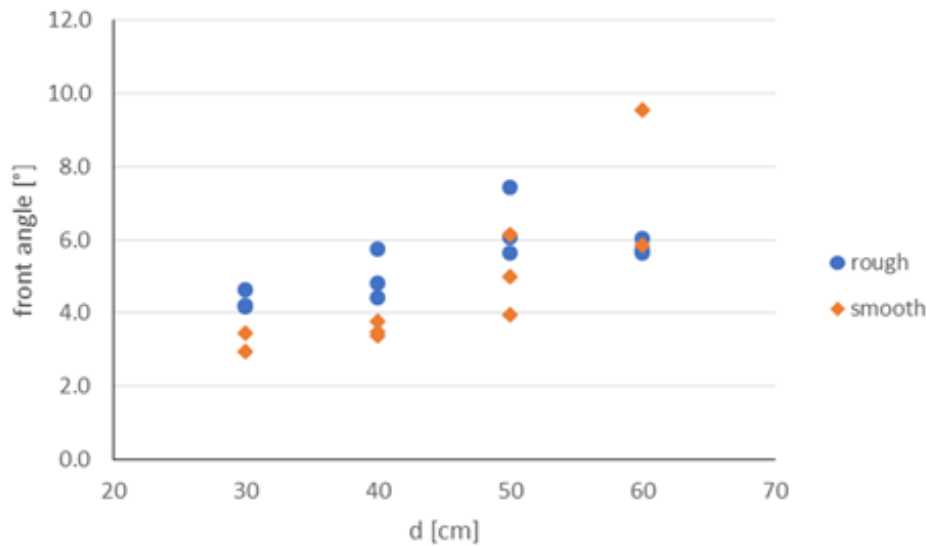
345 clearly different, as shown in Fig. 7. This indicates that the bore front slows down and
 346 steepens up due to the roughness. There are indications that the lower Froude numbers of the
 347 rough bed experiments are more realistic than those of the smooth bed, according to
 348 Glasbergen (2018) and Matsutomi et al. (2001). The SWASH simulations conducted by
 349 Glasbergen (2018) indicate that in the coastal area (around 300-500m from the seashore) the
 350 Fr number for a tsunami-like propagating front should be in the order of 1. Matsutomi et al.
 351 (2001) summarized Froude numbers for past tsunami events, which they calculated using the
 352 surveyed flow depths and velocities estimated from Bernoulli's equation, and showed that
 353 they ranged from 0.7 to 2.0 near the shoreline.



354
 355 Figure 7. Comparison of Fr numbers of rough and smooth bed experimental conditions for
 356 the range of experimental conditions provided in Table 1.

357

358 In order to get a more direct view on the change in bore shape due to the roughness, the slope
 359 of the wave front was measured from the video images that were recorded during the tests.
 360 The image taken at the moment that the front made first contact with the wall was used for the
 361 analysis. Then, the water depth of the wave at a distance of 30 cm from the wall was read
 362 from the image. The water surface could be distinguished best by observing a series of
 363 pictures from the movie recording, with the image coordinates being transformed into real-life
 364 coordinates by relating the pixel size to objects of known size in the image (that were located
 365 at the same distance from the camera as the water surface). The pixel size ranged from 0.5 to
 366 1 mm. No image correction was applied, so that the accuracy was estimated to be better than
 367 5%. From Figure 8 it can be seen that the front slope of the wave on the rough bed seems to
 368 be steeper than that on the smooth bed. The only cases in which this trend is not clear are for
 369 the tests with the largest initial water level ($d = 60$ cm).



370

371 Figure 8. Comparison of direct video measurement of front slope angle for smooth and rough
 372 beds, for different water depths (d) in the reservoir.

373

374 3.3. Inundation height after the structure

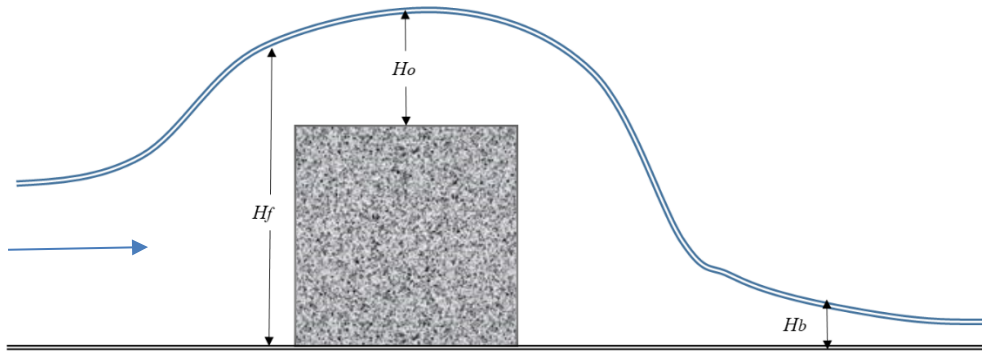
375

376 Esteban et al. (2017) introduced a number of parameters to analyse the wave overtopping. H_f ,
 377 H_o and H_b are the maximum values of the water surface elevation of the bore as it impacts,
 378 overtops and continues to run behind the structure (which were obtained from WG3, WG5
 379 and WG6, respectively). These parameters are diagrammatically explained in Fig. 9. All
 380 experiments showed a similar pattern, with the front rapidly approaching the structure and
 381 eventually overtopping it if they had enough kinetic energy. A quasi-stationary overtopping
 382 flow was subsequently achieved (with the durations indicated by $T/2$ earlier), which would
 383 last several minutes for the case of real tsunamis, though in the case of the laboratory water
 384 quickly ran out.

385

386

387



388

389 Figure 9. Wave parameters used to analyse the overtopping wave. H_f , H_o and H_b represent
 390 maximum values of the surface profile of the wave as it impacts, overtops and runs past the
 391 wall. These values were obtained from WG3, WG5 and WG6, respectively.
 392

393

394 In basic wave hydraulics the energy of an incoming steady flow traversing WG5 without
 395 structure would be given by equation (2)

396

$$397 \quad E_i = \frac{V_i^2}{2g} + H_i \quad (2)$$

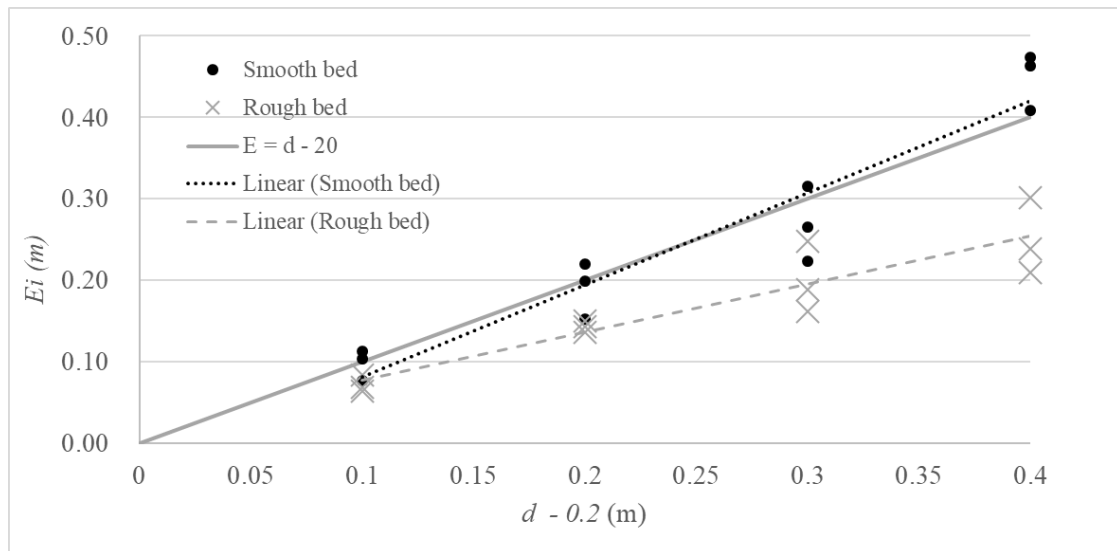
398

399 where E_i is the total head, V_i is the flow velocity (for which we here take the maximum
 400 incident bore front velocity in front of the structure), g is the acceleration due to gravity, and
 401 H_i is the water level (for which we here take the maximum incident water level relative to the
 402 flume false bottom, as defined in Figs. 4).

403

404 The authors first summarized the data for the high wall case (which was not overtopped and
 405 can hence be regarded as the maximum run-up), by using the maximum value recorded at
 406 WG3, placed close to the front of the high seawall, which is referred to as H_{f0} . It is assumed
 407 that H_{f0} is a stagnation pressure that is equal to the incoming ‘energy head’ E_i , which was also
 408 corroborated by Esteban et al. (2017). Fig.10 shows the relationship between static head at the
 409 edge of the gate relative to the elevation of the false bottom ($d - 0.2 \text{ m}$) and E_i , showing how
 410 the rough bed dissipates some of the energy of the incoming wave.

411



412

413 Figure 10. Relationship between E_i and static head at the edge of the gate for the high seawall

414

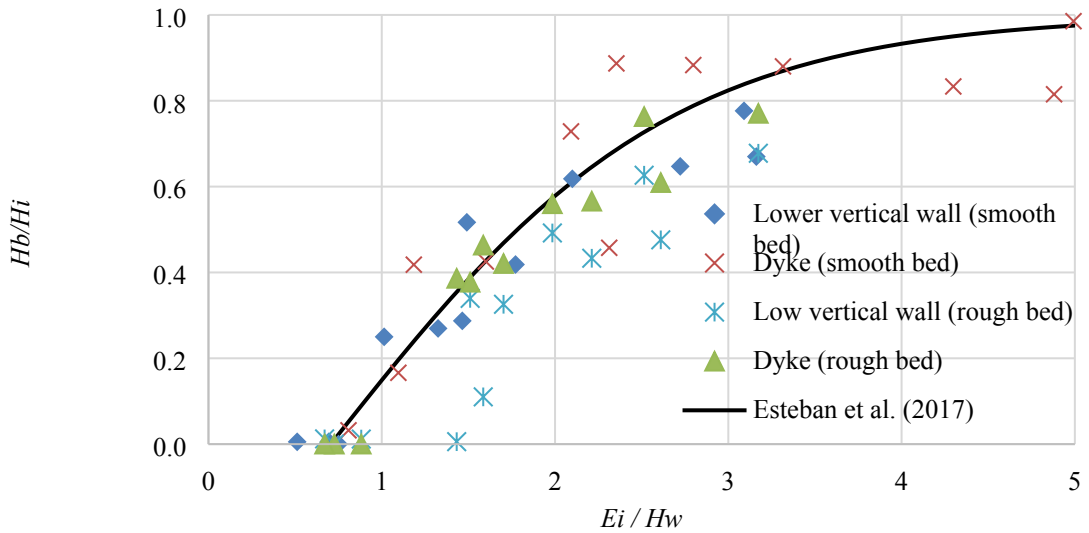
415 Esteban et al. (2017) provide a formula to estimate the inundation height after a structure of a
 416 given height H_w , given the total head of the incident front E_i (which can be calculated
 417 according to its incident wave front velocity V_i and wave height H_i). The ratio H_b / H_i is given
 418 by the relationship between the ratio of wave depth after the wall [H_b] to the incident wave
 419 height [H_i] and the E_i / H_w

420

$$H_b/H_i = \tanh \left(0.51 \frac{E_i}{H_w} - 0.36 \right) \quad (R^2 = 0.89) \quad (3)$$

421

422 The formula is applicable for both dykes and vertical walls, for structures and tsunamis where
 423 $0.2 < H_i/H_w < 1.3$. In the present work the authors verified that the equation is still applicable
 424 for rough beds, and that its range of applicability is independent of the roughness of the bed or
 425 Froude number of the bore, as shown in Fig. 11.



426

427 Fig.11. Relationship between the ratio of wave depth after the wall [H_b] to the incident wave
 428 height [H_i] and the E_i / H_w

429

430

431 3.4. Comparison of results with the ASCE 7 energy gradeline method

432

433 The ASCE7 (ASCE 2016) contains a simplified method (called the Energy Grade Line, or
 434 EGL, method) to establish maximum tsunami inundation depth and flow speed values, based
 435 on inundation maps throughout the United States. As explained in detail in Kriebel et al.
 436 (2017), the EGL assumes that a conservative way to calculate the maximum inundation depth
 437 and flow speed values along a 1-dimensional transect normal to the shoreline is via the total
 438 head equation (2), starting at the point of maximum runup (known elevation and zero kinetic
 439 head), and calculating back towards the shoreline. Moving towards the shoreline, the friction
 440 loss is added back into the total head (5) via Manning's equation (6)

441

$$442 \quad E_i = E_{i-1} + s_i \Delta x \quad (4)$$

$$443 \quad s_i = \frac{u_i^2}{\left(\frac{1}{n}\right)^2 h_i^{\frac{4}{3}}} \quad (5)$$

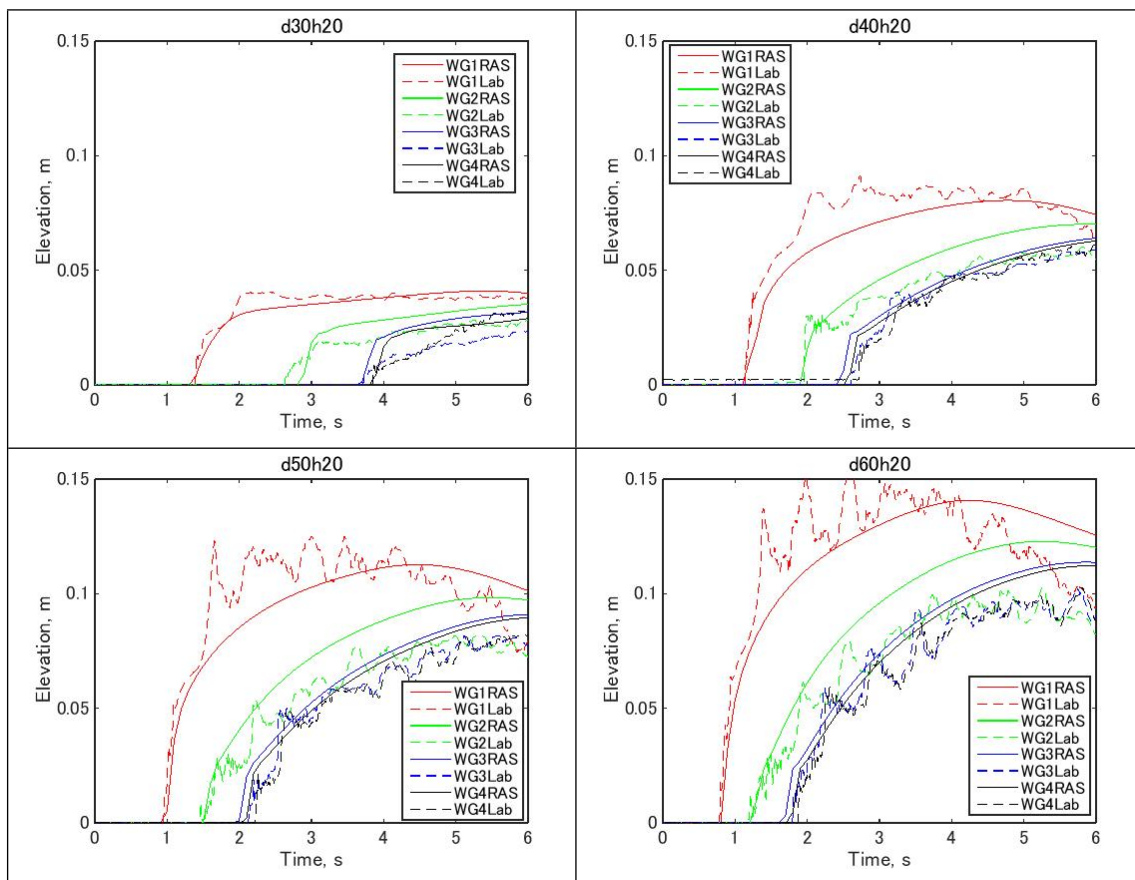
444

445 where s is frictional head loss slope, E is total head, Δx is the distance between calculation
 446 points i and $i-1$, u_i is the maximum flow speed at point i , n is Manning's n , and h_i is maximum
 447 flow depth at point i .

448

449 The experiments of this paper provide a chance to check the Manning's n values suggested by
 450 ASCE7 for Equation (6) against physical results. To do this, a simple HEC-RAS version 5.0.6
 451 unsteady flow model (Bruner, 2016), which uses the one-dimensional St. Venant equations,
 452 was implemented to estimate flow depths and speeds throughout the flume. HEC-RAS has
 453 been shown to model 1-dimensional dam breaks with enough accuracy for practical
 454 applications (Bricker et al., 2017). The model was set up to run with a cross-section spacing
 455 of 1 cm, and a time step of 0.1 sec. Initial conditions represented the water levels within and
 456 in front of the reservoir, and the gate was assumed to open instantaneously, with an orifice
 457 coefficient of 0.8. Since HEC-RAS assumes a rough bed, it was compared only to the rough
 458 bed experiments detailed earlier in this paper. Model calibration resulted in a Manning's
 459 $n=0.03 \text{ s/m}^{1/3}$ (model scale) best approximating the bore speed and depth at each wave gauge.
 460 Fig. 12 shows the comparison of water depth time series at each wave gauge.

461



462 Figure 8.12. Comparison of laboratory experiments (rough bed, no structure scenarios) and
 463 HEC-RAS time series (with $n=0.03 \text{ sm}^{-1/3}$) at wave gauges WG1 through WG4, for reservoir
 464 depths d of 30 cm, 40 cm, 50 cm, and 60 cm, released into a water depth in front of the
 465 reservoir h of 20 cm.

466

467 The lesson from these laboratory experiments is related to the Manning's n values in Eq. (6),
 468 for which ASCE7 recommends values of $0.025 \text{ sm}^{-1/3}$ for "coastal water or nearshore bottom
 469 friction, or open land or fields", $0.04 \text{ sm}^{-1/3}$ for urban areas, and $0.03 \text{ sm}^{-1/3}$ for all other cases.
 470 For coastal and open areas, these suggested values are similar to those for steady flow (i.e.,
 471 Chow, 1959), but for urban and vegetated areas, much larger values are suggested for both
 472 steady and unsteady flows (Bricker et al., 2015). The rough bed laboratory experiments
 473 presented in this research utilized stones 3-5mm in diameter (d_{50} approximately 4mm).
 474 Limerinos (1970) relates the median stone diameter d_{50} and the hydraulic radius R to
 475 Manning's n in steady flow via Eq. (7).

476

$$477 \quad \frac{n}{R^{1/6}} = \frac{0.0926}{0.35 + 2.0 \log_{10} \left(\frac{R}{d_{50}} \right)} \quad (6)$$

478

479 For the shallow, wide flume, the hydraulic radius is approximately equal to the flow depth,
 480 which for the bores shown in Fig. 12 is on the order of 0.05 m. The resulting Manning's n
 481 from Eq. (76), intended for steady flow, is $0.02 \text{ sm}^{-1/3}$. However, the calibrated HEC-RAS
 482 model required $n = 0.03 \text{ sm}^{-1/3}$ to correctly capture the waveforms of Fig. 12, indicating that
 483 the steady-flow Manning's n value was too small for the unsteady dam-break flow of the
 484 experiments. Bricker et al. (2015) suggests that tsunamis require larger effective Manning's n
 485 values than steady flow because of [the](#) enhanced turbulent dissipation of energy in the
 486 unsteady flow bottom boundary layer (Bricker et al., 2005); [Williams and Fuhrman \(2016\)](#)
 487 [and Larsen and Fuhrman \(2019b\) corroborate this further by showing the bottom boundary](#)
 488 [layer under a tsunami to be unsteady, therefore not reaching the full water depth.](#) Since
 489 Manning's n scales with the geometric scale to a power of 1/6, the Manning's n value
 490 expected for a tsunami over this terrain at prototype scale [\(the bed grains themselves](#)
 491 [correspond to cobbles of 20 cm diameter at prototype scale\)](#) is $n = 0.06 \text{ sm}^{-1/3}$, which is again
 492 much larger than any of the Manning's n values suggested by ASCE7 [\(ASCE 7 suggests a](#)
 493 [maximum value of \$n = 0.04 \text{ sm}^{-1/3}\$, for "buildings of at least urban density", which are much](#)
 494 [larger than cobbles\).](#)

495

496 Since the suggested application of Eq. (5) and Eq. (6) in the EGL method is to begin at the
 497 location of runoff (the edge of inundation) on a hazard map, and then to calculate total head E_i
 498 seaward up to the shoreline, the incremental friction head s_i (Eq. (6)) is added back into the
 499 total head each spatial step. Small values of Manning's n generate small values of the friction
 500 head s_i , and thus small values of the total head, with error accumulating seaward. Since the
 501 Manning's n values suggested by ASCE7 are much smaller than those suggested by Bricker

502 et al. (2015) in urban and vegetated areas, the current EGL method appears non-conservative,
503 requiring further research into appropriate Manning's n values for tsunamis.

504

505

506

507 **4. DISCUSSION**

508 The experiments detailed in this study, combined with the HEC-RAS computer simulations,
509 and those performed by Glasbergen (2018) allowed the authors to obtain some insights into
510 how accurately the laboratory experiments can represent tsunami waves.

511

512 The roughness of the experiment bed used has a clear influence on the incoming tsunami front.

513 The shape of the ~~is-waves~~ ~~was~~are different, with steeper fronts and lower Froude numbers for
514 rough bed experiments. However, the different approaching flows did not noticeably change
515 the observed response of the tested tsunami walls to the transient flow. The overtopping flow
516 depth data collapsed onto the results of Esteban et al. (2017) for smooth walls, and provides
517 further evidence that the equation of Esteban et al. (2017) might be applicable to realistic
518 tsunamis. It also is further proof that the total head is a good parameter to describe the
519 hydraulic response of the structure to the considered stationary/transient flow (while formally
520 it is only valid for stationary flow). Herewith, the range of applicability of the formula has
521 been increased to encompass a wider range of conditions.

522

523 The simulation of tsunamis in the laboratory is clearly difficult, as Froude numbers should
524 match those of the real tsunamis. Glasbergen (2018) computed tsunami generation and runup
525 for realistic ranges of tsunami sources and coastal shapes, using the model SWASH (Zijlema
526 et al., 2011). After calibration of the inundation depth and the runup height at the coast near
527 the town of Yuriage, it was found that a Manning's n of $0.06 \text{ sm}^{-1/3}$ could reproduce the event
528 well. Glasbergen (2018) then determined (slightly differently defined) Froude numbers for the
529 bore fronts that resulted from these tsunamis, and compared them to the smooth bed tests
530 (Esteban et al., 2017). For the smooth bed tests the bore-front Froude numbers at the location
531 of the structure ranged from 1.45 to 2.69 while the bore-front Froude numbers of the
532 simulations were much lower at that location (ranging from 0.65 to 1.14). However, the
533 computed bore-front Froude numbers at the coast were 1.34 to 2.6, so essentially the inland
534 bore-front Froude numbers (by Glasbergen, 2018) of the smooth bed tests match the Froude
535 numbers of the simulations at the coast line. With the increased roughness the bore slows

536 down and steepens, and this Froude number resembles the inland bore front-Froude number
537 more closely.

538

539 A HEC-RAS simulation calibrated to the rough-bed laboratory experiments results in a
540 Manning's n much higher than that suggested by ASCE7. The implications of this for disaster
541 risk management are that the ASCE7 energy grade line (EGL) method is non-conservative.
542 This is because the friction loss in (Equation 6), when added back into Equation (5) between
543 the inundation limit and the shoreline, is smaller than the actual friction loss. However, for the
544 USA this error may be mitigated since the original simulations used to generate the ASCE7
545 tsunami inundation maps also used Manning's n values that were too small, thereby resulting
546 in conservative estimates for the limit of the inundation itself. A real danger is that the
547 ASCE7 method may be applied by non-US entities looking to use the EGL method with
548 hazard maps that were not generated in the same way as the ASCE7 hazard maps. If the EGL
549 method is applied with inundation maps based on historical data, for example, the resulting
550 flow depths and speed estimated by the EGL method would be too small. This is particularly
551 worrying, given that the product of these two parameters largely determines mortality rates
552 (with depth velocity products of over $1.2 \text{ m}^2/\text{s}$ generally considered as the upper limit for
553 pedestrians, Suga et al., 1995, Wright et al., 2010, Takagi et al., 2016).

554

555 The results of the present experiments thus emphasize the need to consider the incident bore
556 velocity in the design of coastal protection structures. Video footage of the *2011 Tohoku*
557 *Earthquake Tsunami* highlighted how in some areas the tsunami manifested itself as rapidly
558 rising tide, in others as a slow bore, and yet in others as a rapidly advancing high velocity
559 bore. This further emphasizes the need to start cataloguing tsunami waves into different types
560 of waves, which should be clearly described and catalogued, rather than simply lumped
561 together under the term "tsunami" (as in, efforts should be made to catalogue tsunami waves
562 into different types, in the same way that breaking wind waves are differentiated into breaking,
563 spilling and surging by the clearly defined Iribarren number, breaking solitary waves are
564 classified by the solitary wave breaking criterion (Grilli et al., 1997), and breaking windwave
565 groups are described by the normalized bed slope parameter (Battjes et al., 2004)).
566 [Glasbergen \(2018\), Roubos \(2019\), and Larsen and Fuhrman \(2019a\) present suggestions for](#)
567 [such a quantitative classification of tsunami wave types.](#) This difference in wave type will
568 have implications for the design of coastal dykes, as under the current tsunami disaster
569 management in Japan (which differentiates Level 1 and 2 events), coastal structures need to
570 protect settlements against the expected inundation that could be brought about as a result of a
571 1 in 100 year tsunami (Level 1). The results in thus indicate that this is not just a problem of

572 how high to build the dyke, but that careful consideration needs to be given to the wave
573 velocity and overtopping mechanism. While consideration of the failure mechanism is outside
574 of the scope of this work, it is worth noting how lessons have been learnt as a consequence of
575 the 2011 event, and that many new structures have improved leeward slope and toe
576 protection[Kato et al., 2012; Mikami et al., 2013; Jayaratne et al., 2016].

577

578

579

580

581 **5. CONCLUSIONS**

582

583 The level of understanding on how to defend against tsunamis has greatly increased in the last
584 15 years, through observations of the aftermaths of the many events that have taken place in
585 this period, and important research efforts have been made with laboratory experiments and
586 computer simulations. Nevertheless, important challenges and gaps in knowledge still exist
587 regarding how to accurately model these waves in the laboratory. In the present work the
588 authors analysed how changes in bed roughness affect a dam-break bores, and the resulting
589 overtopping processes on three different structures, namely an “infinite” vertical wall, a dyke,
590 and a low vertical wall.

591

592 The bores on rough floors had lower Froude numbers and steeper fronts. As a result, the range
593 of applicability of the formula for overtopping flow depth by Esteban et al. (2017) has been
594 increased to encompass this different type of rough-floor approach flow.

595

596 The results clearly corroborate the necessity of considering the energy present in the bore to
597 determine whether a structure will be overtopped or not, which is a critical consideration
598 considering how coastal structures in Japan should not be overtopped by a 1 in 100 tsunami
599 event (Level 1). They also show the importance of clearly modelling the velocity and Froude
600 number of a tsunami, and the importance of conducting experiments using a realistic rough
601 bed, for which a suitable Manning’s n ~~seems to be around~~ was $0.06 \text{ sm}^{-1/3}$ for both our
602 experiments (which correspond to a bed of cobbles at prototype scale) and for a SWASH
603 model calibrated by Glasbergen (2018) for the tsunami inundation of Yuriage in 2011.
604 Otherwise, the use of a smooth bed in tsunami experiments might result in waves that do not
605 accurately reproduce the real phenomena observed in nature (though the present experiments
606 also indicate that they would represent conservative estimates, as compared to rough beds)

607

608

609

610 **Acknowledgements**

611 The present work was performed as a part of activities of
612 Research Institute of Sustainable Future Society, Waseda Research Institute
613 for Science and Engineering, Waseda University. The authors would also like to appreciate
614 the support of the Japanese Ministry of Education (Mombukagakusho), and the Graduate
615 Program on Sustainability Science, Global Leadership Initiative (GPSS-GLI). The laboratory
616 experiments were also financially supported by the Strategic Research Foundation Grant-
617 aided Project for Private Universities from the Japanese Ministry of Education, Culture,
618 Sports, Science and Technology to Waseda University (No. S1311028) (Tomoya Shibayama).
619 TU Delft participation was funded by the Delta Infrastructure and Mobility Initiative [DIMI]
620 and the Erasmus+ Master of Science in Marine Engineering and Management (CoMEM)
621 program.

622

623

624 **REFERENCES**

625

626 ASCE (2016) ASCE 7 Standard, Minimum Design Loads and Associated Criteria for
627 Buildings and Other Structures ASCE7-16. Chapter 6 – Tsunami Loads and
628 Effects. American Society of Civil Engineers.

629 Battjes, J. A., Bakkenes, H. J., Janssen, T. T., & Van Dongeren, A. R. (2004).
630 Shoaling of subharmonic gravity waves. *Journal of Geophysical Research:*
631 *Oceans*, 109(C2).

632 Bricker, J. D., Inagaki, S., & Monismith, S. G. (2005). Bed drag coefficient variability
633 under wind waves in a tidal estuary. *Journal of Hydraulic Engineering*, 131(6),
634 497-508.

635 Bricker, J. D., Francis, M., & Nakayama, A. (2012). Scour depths near coastal
636 structures due to the 2011 Tohoku Tsunami. *Journal of Hydraulic*
637 *Research*, 50(6), 637-641.

638 Bricker, J. D., Gibson, S., Takagi, H., & Imamura, F. (2015). On the need for larger
639 Manning's roughness coefficients in depth-integrated tsunami inundation
640 models. *Coastal Engineering Journal*, 57(02), 1550005.

- 641 Bricker, J. D., Schwanghart, W., Adhikari, B. R., Moriguchi, S., Roeber, V., & Giri,
642 S. (2017). Performance of models for flash flood warning and hazard assessment:
643 The 2015 Kali Gandaki landslide dam breach in Nepal. *Mountain research and
644 development*, 37(1), 5-16.
- 645 Bruner, G. W. (2016). HEC-RAS River Analysis System Hydraulic Reference
646 Manual CPD-69. US Army Corps of Engineers, Hydraulic Engineering
647 ~~Center~~Centre, 8-12.
- 648 Chanson, H. (2006) “Analytical solutions of laminar and turbulent dam break wave,”
649 in R.M.L. Ferreira, E.C.T.L. Alves, J.G.A.B. Leal, and A.H. Cardoso eds. *Proc.
650 Int. Conf. Fluvial Hydraulics River Flow 2006*, Vol. 1: Taylor & Francis Groupe,
651 London, pp. 465– 474. (ISBN:0-415-40815-6).
- 652 Chock, G. (2015) The ASCE7 Tsunami Loads and Effects Design Standard for the
653 U.S. In *Handbook of Coastal Disaster Mitigation for Engineers and Planners*.
654 Esteban, M., Takagi, H. and Shibayama, T. (eds.). Butterworth-Heinemann
655 (Elsevier), Oxford, UK
- 656 Chow, V.T. (1959). *Open Channel Hydraulics*. McGraw-Hill Book Company, New
657 York. 680p.
- 658 Cyranoski D. After the deluge: Japan is rebuilding its coastal cities to protect people
659 from the biggest tsunamis, *Nature*, Vol. 483, pp. 141-143, 2012
- 660 Dressler, R. F. [1954] Comparison of theories and experiments for hydraulic dam-
661 break wave. *Int. Assoc. Sci. Pubs*, Vol. 38, No. 3, pp. 319-328.
- 662 Esteban, M., Danh Thao, N., Takagi, H. and Shibayama, T. [2009]. Pressure Exerted
663 by a Solitary Wave on the Rubble Mound Foundation of an Armoured Caisson
664 Breakwater, 19th International Offshore and Polar Engineering Conference,
665 Osaka.
- 666 Esteban, M., Glasbergen, T., Takabatake, T., Hofland, B., Nishizaki, S., Nishida, Y.,
667 Stolle, J., Nistor, I., Bricker, J., Takagi, H. & Shibayama, T. [2017] “Overtopping
668 of Coastal Structures by Tsunami Waves”. *Geosciences*, 7(4), 121.
669 [doi:10.3390/geosciences7040121]
- 670 Esteban, M., Morikubo, I., Shibayama, T., Aranguiz Muñoz, R., Mikami, T., Danh
671 Thao, N., Ohira, K. and Ohtani, A. [2012a]. Stability of Rubble Mound

- 672 Breakwaters against Solitary Waves”, Proc. of 33rd Int. Conf. on Coastal
673 Engineering, Santander, Spain.
- 674 Esteban, M., Takagi, H. and Shibayama, T. [2012b]. “Modified Goda Formula to
675 Simulate Sliding of Composite Caisson Breakwater”, Coastal Engineering Journal
676 [accepted].
- 677 Esteban, M. Jayaratne, R., Mikami, T., Morikubo, I., Shibayama, T., Danh Thao, N.,
678 Ohira, K., Ohtani, A., Mizuno, Y., Kinoshita, M. and Matsuba, S. [2014]
679 “Stability of Breakwater Armour Units Against Tsunami Attack”, Journal of
680 Waterways, Ports, Coastal and Ocean Engineering, 140:188-198
- 681 Esteban, M., Onuki, M., Ikeda, I and Akiyama, T. (2015) “Reconstruction Following
682 the 2011 Tohoku Earthquake Tsunami: Case Study of Otsuchi Town in Iwate
683 Prefecture, Japan” in Handbook of Coastal Disaster Mitigation for Engineers and
684 Planners. Esteban, M., Takagi, H. and Shibayama, T. (eds.). Butterworth-
685 Heinemann (Elsevier), Oxford, UK
- 686 Estrade, J., & Martinot, A. (1964). Ecoulement consecutif a la suppression dun barrage
687 dans un canal horizontal de section rectangulaire. Comptes Rendus
688 Hebdomadaires des Seances de L’Acadmie Des Sciences, 259(25), 4502 (in
689 french).
- 690 EERI: Earthquake Engineering Research Institute Special Earthquake Report (2011)
691 Learning from Earthquakes: The Tohoku, Japan, Tsunami of March 11, 2011:
692 Effects on Structures, 14pp.
- 693 Fujii, Y., Satake, K., Sakai, S., Shinohara, M. and Kanazawa, T. [2011] Tsunami
694 source of the 2011 off the Pacific coast of Tohoku Earthquake. Earth Planets
695 Space, 63, 815-820.
- 696 Goseberg, N., Wurpts, A. & Schlurmann, T. [2013] “Laboratory-scale generation of
697 tsunami and long waves,” *Coastal Eng.* **79**, 57tal
- 698 Glasbergen, T. (2018) Parameters of incoming tsunami bores for the design of coastal
699 defence structures. Master Thesis, TUDelft.
700 [https://repository.tudelft.nl/islandora/object/uuid%3Aad229966-5403-432d-9a13-](https://repository.tudelft.nl/islandora/object/uuid%3Aad229966-5403-432d-9a13-84a9e7fdb5bc?collection=education)
701 [84a9e7fdb5bc?collection=education](https://repository.tudelft.nl/islandora/object/uuid%3Aad229966-5403-432d-9a13-84a9e7fdb5bc?collection=education)
- 702 Grilli, S. T., Svendsen, I. A., & Subramanya, R. (1997). Breaking criterion and
703 characteristics for solitary waves on slopes. Journal of waterway, port, coastal,
704 and ocean engineering, 123(3), 102-112.

- 705 Hanzawa M, Matsumoto A and Tanaka H [2012] “Stability of Wave-Dissipating
706 Concrete Blocks of Detached Breakwaters Against Tsunami”. Proc. of the 33rd
707 Int. Conference on Coastal Engineering [ICCE]
- 708 Hunt-Raby, A., Borthwick, A.G.L., Stansby, P.K. & Taylor, P.H. (2011)
709 Experimental measurement of focused wave group and solitary wave overtopping.
710 Journal of Hydraulic Research 49(4): 450-464.
- 711 Ikeno, M., Mori, N. and Tanaka, H. [2001]. Experimental Study on Tsunami force
712 and Impulsive Force by a Drifter under Breaking Bore like Tsunamis,
713 Proceedings of Coastal Engineering, JSCE, Vol. 48, pp. 846-850.
- 714 Ikeno, M. and Tanaka, H. [2003]. Experimental Study on Impulse Force of Drift Body
715 and Tsunami Running up to Land, Proceedings of Coastal Engineering, JSCE,
716 Vol. 50, pp. 721-725.
- 717 Iwate Prefecture Tsunami Disaster Prevention Technical Committee [2013] Reference
718 materials #1. Available at
719 <https://www.pref.iwate.jp/area/shingikai/kendo/tsunami/023437.html>. Accessed
720 08 April 2019.
- 721 Jayaratne, M. P. R., Premaratne, B., Adewale, A., Mikami, T., Matsuba, S. Shibayama,
722 T., Esteban, M. and Nistor, I. [2016] “Failure Mechanisms and Local Scour at
723 Coastal Structures Induced by Tsunami”, Coastal Engineering Journal 58 [04]
- 724 Jonkman, S.N. and Penning-Roswell, E. [2008] Human instability in flood flows.
725 Journal of the American Water Resources Association, 44[5]:1208-1218.
- 726 Kato, F., Suwa, Y., Watanabe, K. and Hatogai, S. [2012]. Mechanism of Coastal Dike
727 Failure Induced by the Great East Japan Earthquake Tsunami. Proc. of 33rd Int.
728 Conf. on Coastal Engineering Santander, Spain.
- 729 Kriebel, D. L., Lynett, P. J., Cox, D. T., Petroff, C. M., Robertson, I. N., & Chock, G.
730 Y. (2017). Energy method for approximating overland tsunami flows. Journal of
731 Waterway, Port, Coastal, and Ocean Engineering, 143(5), 04017014.
- 732 Latcharote, P., Suppasri, A., Hasegawa, N., Takagi, H., Imamura, F., [2016] Effect of
733 Breakwaters on Reduction of Fatality Ratio during the 2011 Great East Japan
734 Earthquake and Tsunami, Journal of Japan Society of Civil Engineers, Ser. B2
735 (Coastal Engineering), 72(2) pp.1591-1596.

- 736 [Larsen, B.E., Fuhrman, D.R., 2019a. Full-scale CFD simulation of tsunamis. Part 1:](#)
737 [Model validation and run-up. Coast. Eng. 151, 22-41.](#)
- 738 [Larsen, B.E., Fuhrman, D.R., 2019b. Full-scale CFD simulation of tsunamis. Part 2:](#)
739 [Boundary layers and bed shear stresses. Coast. Eng. 151, 42-57.](#)
- 740 Limerinos, J.T. [1970]. Manning coefficient from measured bed roughness in natural
741 channels. US Geological Survey Water Supply Paper 1898-B.
- 742 Madsen, P. A., Furhman, D. R. and Schaffer, H. A., [2008] On the solitary wave
743 paradigm for tsunamis. Journal of Geophysical Research, 113, C12012.
- 744 Matsutomi, H., Shuto, N., Imamura, F., Takahashi, T. [2001] Field Survey of the 1996
745 Irian Jaya Earthquake Tsunami in Biak Island, Natural Hazards, 24(3), pp. 199-
746 212.
- 747 Mikami, T., Shibayama, T., Esteban, M. and Matsumaru, R. [2012]. Field Survey of
748 the 2011 Tohoku Earthquake and Tsunami in Miyagi and Fukushima Prefectures,
749 Coastal Engineering Journal, Vol. 54, No. 1, pp. 1-26.
- 750 Mikami T., Matsuba S and Shibayama T [2014] Flow Geometry Of Overflowing
751 Tsunamis Around Coastal Dykes, Coastal Engineering Proceedings 2014.
752 Available at:
753 https://journals.tdl.org/icce/index.php/icce/article/view/7615/pdf_839. Accessed
754 [01 June 2016](#).
- 755 MLIT [Ministry of Land, Infrastructure, Transport, and Tourism] [2011].
756 Comprehensive tsunami countermeasures in ports [interim report]. Available at:
757 <http://www.mlit.go.jp/common/000149434.pdf>. Accessed 20 September 2015.
- 758 Mizutani, S. and Imamura, F. [2000]. Hydraulic Experimental Study on Wave Force
759 of a Bore Acting on a Structure, Proceedings of Coastal Engineering, JSCE, Vol.
760 47, pp. 946-950.
- 761 Mori, N. and Takahashi T. [2012]. The 2011 Tohoku Earthquake Tsunami Joint
762 Survey Group [2012] Nationwide Survey of the 2011 Tohoku Earthquake
763 Tsunami, Coastal Engineering Journal, Vol.54, Issue 1, pp.1-27.
- 764 Nandasena, N.A.K, Sasaki, Y. and Tanaka, N. (2012) Modelling field observations of
765 the 2011 Great East Japan tsunami: Efficacy of artificial and natural structures on
766 tsunami mitigation. Coastal Engineering 67, 1-13.

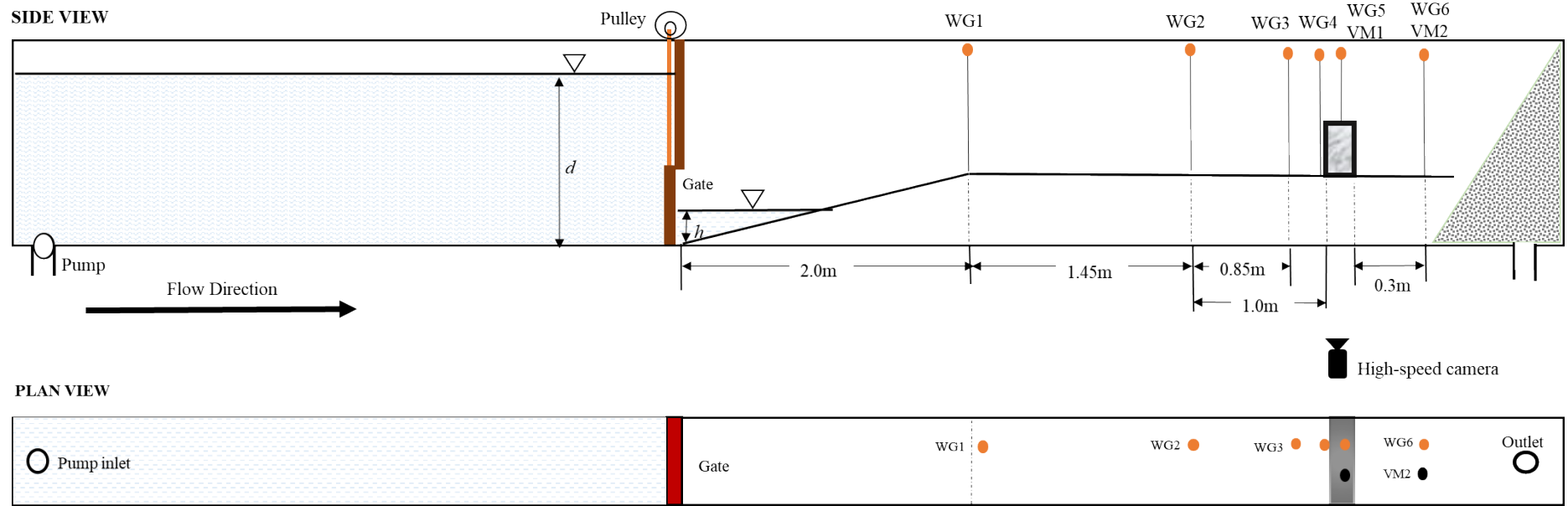
- 767 Nateghi, R., Bricker, J. D., Guikema, S. D., & Bessho, A. (2016). Statistical analysis
768 of the effectiveness of seawalls and coastal forests in mitigating tsunami impacts
769 in Iwate and Miyagi prefectures. *PloS one*, 11(8), e0158375.
- 770 Omira, R., Baptista, M. A., Leone, F., Matias, L., Mellas, S., Zourarah, B., Miranda,
771 J.M. Carrilho, F. and Chereil, J. P. (2013) Performance of coastal sea-defence
772 infrastructure at El Jadida (Marocco) against tsunami threat: lessons learned from
773 the Japanese 11 March tsunami. *Natural Hazards Earth Systems Science*, 13,
774 1779-1794.
- 775 Okumura, N., Jonkman, S., N., Esteban, M., Hofland, B. and Shibayama, T. [2017]
776 “A method for tsunami risk assessment - a case study for Kamakura, Japan”
777 *Natural Hazards*, DOI 10.1007/s11069-017-2928-x
- 778 Ranghieri F and Ishiwatari M [2014] Megadisasters. Lessons from the Great East
779 Japan Earthquake. Available at:
780 [https://openknowledge.worldbank.org/bitstream/handle/10986/.../9781464801532.p](https://openknowledge.worldbank.org/bitstream/handle/10986/.../9781464801532.pdf)
781 [df](https://openknowledge.worldbank.org/bitstream/handle/10986/.../9781464801532.pdf), Accessed 11 July 2016.
- 782 [Roubos, J \[2019\]. Prediction of the characteristics of a tsunami wave near the Tohoku](#)
783 [coastline. Master thesis, TU Delft.](#)
784 [https://repository.tudelft.nl/islandora/object/uuid%3A421cd6b8-fd31-424a-aa9b-](https://repository.tudelft.nl/islandora/object/uuid%3A421cd6b8-fd31-424a-aa9b-529dc17018eb?collection=education)
785 [529dc17018eb?collection=education](https://repository.tudelft.nl/islandora/object/uuid%3A421cd6b8-fd31-424a-aa9b-529dc17018eb?collection=education)
- 786 San Carlos-Arce, R., Onuki, M., Esteban, M. and Shibayama, T. [2017] “Risk
787 Awareness and Intended Tsunami Evacuation Behaviour of International Tourists
788 in Kamakura City, Japan”. *International Journal of Disaster Risk Reduction* 23,
789 178-192.
- 790 Sakakiyama, T. [2012]. Stability of Armour Units of Rubble Mound Breakwater
791 against Tsunamis, Proc. of 32nd Int. Conf. on Coastal Engineering, Santander,
792 Spain.
- 793 Shibayama, T., Esteban, M., Nistor, I., Takagi, H., Danh Thao, N., Matsumaru, R.,
794 Mikami, T., Aranguiz, R., Jayaratne, R. and Ohira, K. (2013) Classification of
795 Tsunami and Evacuation Areas, *Journal of Natural Hazards*, 67 (2), 365-386
- 796 Stansby, P., Xu, R. Rogers, B.D., Hunt-Raby, A., Borthwick, A.G.L. and Taylor, P.H.
797 (2008) Modelling overtopping of a sea defence by shallow-water Boussinesq,
798 VOF and SPH methods. Proc. of Flood Risk Assessment Conference, Oxford.

- 799 Stolle, J., Stolle, J., Krautwald, C., Robertson, I., Achiari, H., Mikami, T.,
800 Nakamura, R., Takabatake, T., Nishida, Y., Shibayama, T., Esteban, M., Nistor,
801 I., and Goseberg, N. (2019) "Engineering Lessons from the 18 September 2018
802 Indonesian Tsunami: Debris Loading", *Canadian Hydraulics Journal*
803 (provisionally accepted)
- 804 Suga, K., Uesaka, T., Yoshida, T., Hamaguchi, K., Chen, Z., 1995. Preliminary study
805 on feasible safe evacuation in flood disaster. *Proc. Hydraul. Eng. JSCE* 39, 879–
806 882.
- 807 Supparsi, A., Koshimura, S., Imai, K., Mas, E., Gokon, H., Muhari, A. and Imamura,
808 F. (2012) Damage characteristic and field survey of the 2011 Great East Japan
809 tsunami in Miyagi Prefecture. *Coastal Engineering Journal*, 54, 1250005.
- 810 Takagi H., Bricker J. Assessment of the effectiveness of general breakwaters in
811 reducing tsunami inundation in Ishinomaki, *Coastal Engineering Journal*, Vol. 56,
812 No. 4, 21p., 2014.
- 813 Tanimoto, L., Tsuruya, K. and Nakano, S. [1984]. Tsunami Force of Nihonkai-Chubu
814 Earthquake in 1983 and Cause of Revetment Damage, *Proceeding of the 31st*
815 *Japanese Conference on Coastal Engineering*, JSCE.
- 816 Takagi, H., Pratama, M. B., Shota, K., Esteban, M., Aranguiz, R., and Ke, B. (2019)
817 "Analysis of generation and arrival time of landslide tsunami to Palu City due to
818 the 2018 Sulawesi Earthquake", *Landslides* (accepted)
- 819 Takabatake, T., Shibayama, T., Esteban, M., Ishii, H. and Hamano, G. [2017]
820 "Simulated Tsunami Evacuation Behaviour of Local Residents and Visitors in
821 Kamakura, Japan". *International Journal of Disaster Risk Reduction* 23, 1-14
- 822 Takabatake, T., Shibayama, T., Esteban, M. & Ishii, H. [2018] "Advanced casualty
823 estimation based on tsunami evacuation intended behavior: case study at
824 Yuigahama Beach, Kamakura, Japan". *Natural Hazards*, 1-26.
825 [doi:10.1007/s11069-018-3277-0]
- 826 Takagi H., Li S., de Leon M., Esteban M., Mikami T., Matsumaru R., Shibayama T.,
827 Nakamura R. (2016) Storm surge and evacuation in urban areas during the peak
828 of a storm, *Coastal Engineering*, Vol. 108, pp. 1-9, DOI:
829 10.1016/j.coastaleng.2015.11.002
- 830 Tomita, T., Yeom, G.S., Ayugai, M., and Niwa, T. [2012]. Breakwater Effects on
831 Tsunami Inundation Reduction in the 2011 off the Pacific Coast of Tohoku

- 832 Earthquake. Journal of the Japan Society of Civil Engineers, series B2 (Coastal
833 Engineering).68(2):I_156-60.
- 834 Tonkin, S. P., Francis, M., & Bricker, J. D. (2014). Limits on Coastal Scour Depths
835 due to Tsunami. In International Efforts in Lifeline Earthquake Engineering (pp.
836 671-678). ASCE.
- 837 US Army Coastal Engineering Research Center [1977] Shore Protection Manual
- 838 Wijetunge, J.J. [2006]. Tsunami on 26 December 2004: Spatial Distribution of
839 Tsunami Height and the Extent of Inundation in Sri Lanka, Science of Tsunami
840 Hazards, Vol. 24, No 3, pp. 225-239.
- 841 [Williams, I.A., Fuhrman, D.R., 2016. Numerical simulation of tsunami-scale](#)
842 [wave boundary layers. Coast. Eng. 110, 17–31.](#)
- 843 Wright, K., Doody, B.J., Becker, J., McClure, J., 2010. Pedestrian and motorist flood
844 safety study: a review of behaviours in and around floodwater and strategies to
845 enhance appropriate behaviour. GNS Science Report 2010/51 (91 pp.).
- 846 Yamao, S., Esteban, M., Yun, N. Y., Mikami, T. and Shibayama, T. (2015)
847 “Estimation of the current risk to human damage life posed by future tsunamis in
848 Japan” in Handbook of Coastal Disaster Mitigation for Engineers and Planners.
849 Esteban, M., Takagi, H. and Shibayama, T. (eds.). Butterworth-Heinemann
850 (Elsevier), Oxford, UK
- 851 Zijlema, M., Stelling, G. and Smit, P., 2011. SWASH: An operational public domain
852 code for simulating wave fields and rapidly varied flows in coastal waters. Coast.
853 Engng., 58, 992-1012.
- 854
- 855

0

856



857

858

859

860

861

862

Figure 3. Schematic of the wave flume and instrumentation [not to scale]

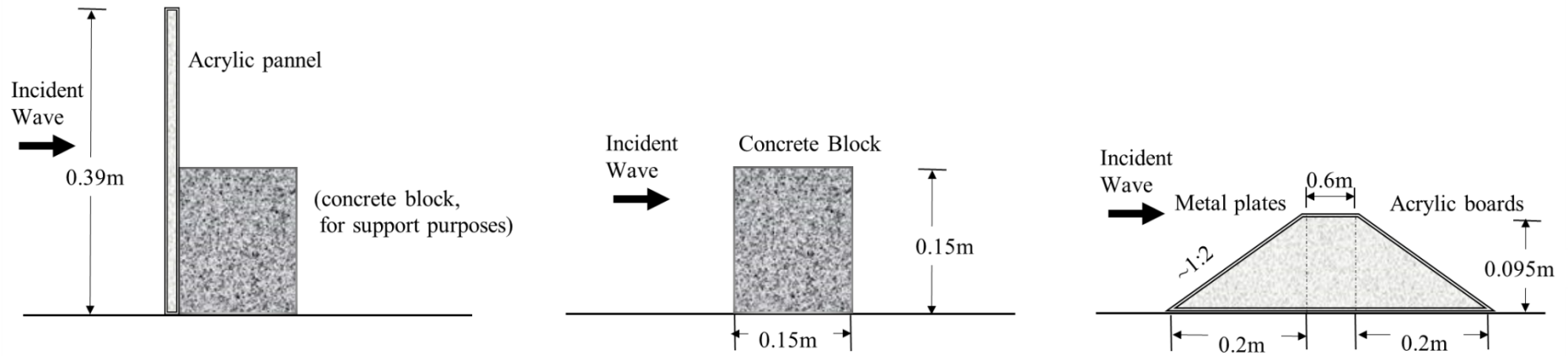


863

864

Figure 4. Experimental Apparatus. a) View of the back of the gate. b) Weight system to release the gate. c) wave gauge and velocity meters (smooth flat bed). d) stone flat bed

865



866
867
868
869
870

Figure 5. The structure types tested [not to scale]. From left to right, “high vertical wall”, “low vertical wall” and dyke.